Intestinal CD4+ T cells treated with *Pseudostellaria heterophylla* polysaccharide improve insulin resistance in BNL CL.2 cells by modulating PI3K/AKT signaling and energy metabolism

YONGJUN KAN[1*], YINGYING LIU[2*], YATING HUANG[3], LI ZHAO[1], JIANG CHANG[1], WENSHENG PANG[3], WENXIONG LIN[4] and JUAN HU[1,2]

[1]Institute of Materia Medica, Fujian Academy of Chinese Medical Sciences, Fuzhou, Fujian 350003, P.R. China; [2]Clinical Research Institute, The Second Affiliated Hospital of Fujian University of Traditional Chinese Medicine, Fuzhou, Fujian 350003, P.R. China; [3]School of Pharmacy, Fujian University of Traditional Chinese Medicine, Fuzhou, Fujian 350122, P.R. China; [4]Fujian Key Laboratory for Agroecological Processes and Safety Monitoring, Fujian Agriculture and Forestry University, Fuzhou, Fujian 350002, P.R. China

Received April 16, 2025; Accepted August 14, 2025

DOI: 10.3892/mmr.2025.13682

Abstract. *Pseudostellaria heterophylla* polysaccharide PF40 has shown potential in alleviating insulin resistance by modulating CD4+ T cells in the intestinal tissue of rats with type 2 diabetes mellitus. To further elucidate the underlying mechanism, CD4+ T cells were isolated from the intestinal tissue of rats treated with PF40 (P-T) and co-cultured with insulin-resistant (IR)-BNL CL.2 cells. Oxidative stress was assessed by measuring reactive oxygen species, malondialdehyde and superoxide dismutase activity, while apoptosis was evaluated by flow cytometry. Insulin sensitivity was examined by glucose uptake and consumption assays. Protein expression related to the PI3K/AKT pathway was determined by western blotting, and targeted energy metabolomics was performed to analyze glycolysis and the tricarboxylic acid cycle. P-T treatment reduced oxidative stress in IR-BNL CL.2 cells by reducing reactive oxygen species and malondialdehyde levels, while increasing superoxide dismutase activity. Additionally, P-T inhibited apoptosis and improved insulin sensitivity, as evidenced by the increased glucose uptake and consumption. Mechanistically, P-T decreased phosphorylated-insulin receptor substrate-1 expression, leading to activation of the PI3K/AKT signaling pathway, which enhanced glucose metabolism. Targeted energy metabolomics analysis further revealed that P-T regulated glycolysis and the tricarboxylic acid cycle, ameliorating energy metabolism dysfunction. Notably, the combined treatment of PF40 and metformin indicated potential synergistic effects. These findings highlight the critical role of intestinal CD4+ T cells in PF40-mediated metabolic regulation, suggesting that targeted modulation of intestinal immune cell homeostasis may offer a promising strategy for the prevention and treatment of insulin resistance.

Correspondence to: Dr Juan Hu, Institute of Materia Medica, Fujian Academy of Chinese Medical Sciences, 2nd Floor, Siyuan Building, 282 Wusi Road, Gulou, Fuzhou, Fujian 350003, P.R. China
E-mail: huj@fjtcm.edu.cn

*Contributed equally

Key words: Pseudostellaria heterophylla, polysaccharides, CD4+ T cells, insulin resistance

Introduction

Insulin resistance represents a fundamental pathophysiological mechanism in the development of type 2 diabetes mellitus (T2DM), characterized by a reduced response of tissue to insulin signaling. Research has demonstrated that intestinal immune system dysregulation, which manifests as persistent inflammation, serves a pivotal role in mediating T2DM-associated insulin resistance (1). Experimental evidence has indicated that aberrant activation of T helper (Th)17 cells triggers intestinal inflammation and precipitates autoimmune disorders, whereas regulatory T cells (Tregs) exert immunosuppressive functions to modulate inflammatory processes (2). Furthermore, perturbation of the homeostatic balance between Tregs and Th17 cells has emerged as a critical determinant in the pathogenesis of insulin resistance, as evidenced by elevated IL-17 levels and enhanced pro-inflammatory cytokine secretion (3). Multiple studies have established that Tregs and Th17 cells are essential mediators in maintaining intestinal immune homeostasis, with their dynamic equilibrium being crucial for proper immune function (4-6).

Pseudostellaria heterophylla (Miq.) Pax ex Pax et Hoffm, formerly known as TaiZiShen, was initially described in the Chinese book Ben Cao Cong Xin, and is often used to treat diabetes, chronic obstructive pneumonia, cardiomyocyte injury, immune deficiency and other diseases (7-9). This herb has been included in the Chinese Pharmacopoeia primarily due to its medicinal value (7).

Polysaccharides (molecular weight: 52-210 kDa), such as PF40, are the primary active ingredient of *Pseudostellaria*

heterophylla (10). Structural elucidation of PF40 by UV spectroscopy, Fourier transform infrared spectroscopy and nuclear magnetic resonance has confirmed the absence of protein and nucleic acid impurities, as well as the presence of characteristic α-pyranose configurations (11). Notably, Congo red assay and scanning probe microscopy analyses have revealed that PF40 adopts a triple-helical conformation and a multi-branched molecular structure, features known to enhance the biological stability and functional activity of polysaccharides. Compared with other plant-derived polysaccharides, PF40 displays superior thermal stability and is predominantly amorphous in physical state, as evidenced by X-ray diffraction analysis. These properties not only support its suitability for pharmaceutical processing but also enhance its *in vivo* functionality (11). A radioisotope tracing study previously demonstrated that PF40 exhibits targeted accumulation in the small intestine following oral administration, suggesting a high degree of intestinal bioavailability and potential for interaction with gut-associated lymphoid tissues (12). This gut-enrichment behavior may explain its previously observed ability to modulate intestinal immune homeostasis, restore Th17 cell/Treg balance, and improve mucosal barrier integrity in diabetic models (9,11). Together, these unique structural and biopharmaceutical features distinguish PF40 from other polysaccharides and support its candidacy as a novel immunomodulatory agent for the treatment of metabolic diseases.

Previous studies have shown that PF40 has favorable pharmacological activity in improving insulin resistance and reducing fasting glucose in a rat model of T2DM (10-12). In our previous study, it was revealed that PF40 can correct imbalances in Treg/Th17 cells in the jejunal tissue (11). Th17 cells and Tregs, alongside Th1 and Th2 cells, constitute crucial subpopulations of $CD4^+$ T lymphocytes that serve key roles in maintaining intestinal microbial balance and overall metabolic homeostasis (13,14). Studies have shown that in states of insulin resistance, pro-inflammatory $CD4^+$ T cells, such as Th1 and Th17 cells, are markedly activated in the gut, whereas anti-inflammatory Tregs are relatively deficient, exacerbating intestinal inflammatory responses (15,16). Additionally, impairment of the intestinal barrier and alterations in gut microbiota composition further amplify the expansion of inflammatory $CD4^+$ T cells, thereby promoting the progression of systemic insulin resistance (17,18). Interfering with the balance of intestinal $CD4^+$ T cell subpopulations may offer a novel approach for preventing and treating insulin resistance. Previous research has suggested that enhancing Treg activity or suppressing the uncontrolled proliferation of Th1 and Th17 cells can notably improve insulin sensitivity and alleviate symptoms of metabolic disorders (19,20). However, understanding regarding how the $CD4^+$ T-cell subset balance influences insulin resistance, and the detailed molecular mechanisms involved, remains limited.

Our previous study established the therapeutic efficacy of PF40 in rat models of T2DM, where dose-response analyses were conducted, and it was demonstrated that PF40 could markedly improve insulin sensitivity and metabolic parameters (10). Notably, when combined with metformin, PF40 exerts a synergistic effect, resulting in superior glycemic control and reduced systemic inflammation compared with either treatment alone (10,11). These findings underscore the potential of PF40 as an effective immunometabolic modulator. Building on this evidence, the present study focuses on identifying the cellular and molecular mechanisms by which PF40 influences hepatocellular insulin signaling via intestinal $CD4^+$ T cells.

The present study aimed to evaluate the activity of differentially treated $CD4^+$ T cells in ameliorating insulin resistance using an *in vitro* cell model. Particular focus was given to their effects on antioxidant activity, apoptosis, glucose uptake and energy metabolism in insulin-resistant (IR) cells, alongside their influence on the insulin receptor substrate-1 (IRS-1)/PI3K/AKT signaling pathway. By elucidating the roles and underlying regulatory mechanisms of differentially treated $CD4^+$ T cells, the current study may provide theoretical support for developing interventional strategies against insulin resistance and advance immunotherapeutic approaches for metabolic diseases.

Materials and methods

Chemicals and materials. Pseudostellaria heterophylla was obtained from a Good Agricultural Practice-certified cultivation base in Zherong (Fujian Zheshen Biotechnology Co., Ltd), and PF40 was prepared as described previously (10). The total sugar content was measured using the anthrone-sulfuric acid method as described previously (21), and the protein content of PF40 was determined using a Bradford assay with BSA (Beyotime Biotechnology) as the standard (22). The average molecular weight of PF40 was characterized by high-performance gel permeation chromatography (23). The monosaccharide composition was analyzed using pre-column derivatization with 1-phenyl-3-methyl-5-pyrazolone followed by high-performance liquid chromatography (HPLC) (24). BNL CL.2 cells were obtained from Procell Life Science & Technology Co., Ltd. Other materials, including fetal bovine serum (FBS), DMEM and trypsin (used for cell passaging), were obtained from Gibco (Thermo Fisher Scientific, Inc.). DMSO was sourced from MilliporeSigma. The glucose assay kit (cat. no. S0201S) was acquired from Shanghai Beyotime Biotechnology. The phosphorylated (p)-PI3K (p85-Tyr607; cat. no. AF3241) polyclonal antibody was purchased from Affinity biosciences Co., Ltd. PI3K (cat. no. A4992), IRS-1 (cat. no. A16902), p-IRS-1 (Ser307; cat. no. AP0552), AKT (cat. no. A17909) and p-AKT (S473; cat. no. AP1208) polyclonal antibodies were obtained from ABclonal Biotech Co., Ltd.

Intervention and purification of $CD4^+$ T cells. The T2DM rat model was established as described previously (11). Briefly, 60 male Sprague Dawley rats (4 weeks, 180-200 g, SPF conditions) were obtained from Shanghai Institutes for Biological Sciences Shanghai Laboratory Animal Center (certificate no. SCXK 2017-0005) and housed under standard conditions with free access to food and water and a 12 h light/12 h dark cycle. Except for the normal control group, all other rats were intraperitoneally injected with freshly prepared STZ solution (0.021 mol/l in pH 4.5 sodium citrate buffer, 0.5 ml/100 g bodyweight) after overnight fasting with free access to water to induce diabetes. After 3 days, rats with fasting blood glucose ≥16.7 mmol/l were considered to have T2DM. A total of 38 rats were successfully rendered

diabetic. These T2DM rats were randomly assigned to four groups: model (n=10), PF40 [1.5 g/kg body weight (bw); n=10], metformin (Merck KGaA; 135 mg/kg bw; n=9) and PF40 + metformin (PF40, 1.5 g/kg bw + metformin 135 mg/kg bw; n=9). Animals received their assigned treatments via oral gavage once daily for a duration of 4 weeks. The normal control group received an equivalent volume of saline. Each intervention lasted 4 weeks in total. Subsequently, the rats were euthanized in a small animal anesthesia machine using 10% isoflurane for 30 min, with death confirmed by the absence of a heartbeat. Jejunal lymphocytes were isolated as described previously (25). Briefly, jejunal tissue was rapidly excised and rinsed with cold PBS to remove feces. The tissue was then minced and digested in a solution containing 50 mg/ml deoxyribonuclease I and 30 mg/ml liberase for 30 min at 37˚C to facilitate lymphocyte release. The digested tissue was filtered through a 70-μm cell mesh to obtain a single-cell suspension, washed with PBS and resuspended in 40% Percoll solution. This suspension was layered over 70% Percoll solution and centrifuged at 800 x g for 15 min at 4˚C. Lymphocytes were collected from the interface between the two layers. $CD4^+$ T cells were then purified from the lymphocyte population using the MagniSort™ $CD4^+$ T Cell Enrichment Kit (Thermo Fisher Scientific, Inc.; cat. no. 8804-6820-74) according to the manufacturer's protocol. Cell purity was assessed using a NovoCyte flow cytometer (NovoCyte; Agilent Technologies, Inc.) and analyzed with NovoExpress software (version 1.4.1; Agilent Technologies, Inc.). Samples in which $CD4^+$ T cells accounted for at least 80% of the population were used for further analysis. $CD4^+$ T cells were labeled based on the interventions the mice received as follows: Control (Con-T), model (Mod-T), PF40 (P-T), metformin (M-T), and combined PF40 and metformin (PM-T). Cells were cultured in DMEM supplemented with 10% FBS and 1% penicillin-streptomycin at 37˚C in a humidified incubator with 5% CO_2.

Establishment of the insulin resistance model. BNL CL.2 cells were seeded in culture flasks and maintained in low-glucose DMEM supplemented with 10% FBS and 1% penicillin-streptomycin at 37˚C in a humidified incubator with 5% CO_2 and 95% humidity. The culture medium was changed every 48 h. Once the cells reached 80-90% confluence, the culture medium was replaced with DMEM containing varying concentrations of insulin ($1x10^{-6}$, $1x10^{-7}$, $1x10^{-8}$ and $1x10^{-9}$ mol/l; Sigma-Aldrich; Merck KGaA; cat. no. Y0001717) and incubated at 37˚C for 24 h to identify the optimal insulin concentration that could induce insulin resistance. Based on glucose measurements in the culture medium, the concentration of $1x10^{-7}$ mol/l was identified as the ideal concentration for inducing insulin resistance. Subsequently, cells were treated with $1x10^{-7}$ mol/l insulin for 24, 36, 48 and 60 h to determine the optimal duration for stable induction of insulin resistance. Untreated cells were used as a control group and each experimental condition included six replicates. After treatment, the supernatant was collected, and the glucose concentration in the culture medium was measured using a glucose assay kit using the o-toluidine method (Beyotime Biotechnology). The glucose consumption was calculated based on the difference between the initial glucose concentration and the post-treatment concentration, enabling assessment of the response of cells to insulin and identification of the optimal concentration and treatment duration for stable insulin resistance induction.

Co-culture of IR-BNL CL.2 cells with $CD4^+$ T cells. The co-culture model was established using the Transwell insert system, with $CD4^+$ T cells seeded in the apical medium and IR-BNL CL.2 cells seeded in the basolateral medium (26,27), using inserts with 6 wells and a pore size of 0.4 μm. Purified $CD4^+$ T cells were co-cultured with IR-BNL CL.2 cells at various $CD4^+$ T cells to IR-BNL CL.2 cell ratios: 1:1, 2:1, 5:1, 10:1, 20:1 and 40:1, to determine the optimal ratio for the co-culture system. Phenol red-free DMEM (Thermo Fisher Scientific, Inc.) was used to avoid color interference. Both $CD4^+$ T cells and IR-BNL CL.2 cells were cultured in this medium, supplemented with 10% FBS, and incubated at 37˚C with 5% CO_2 for 24 h. After 24 h, 10 μl CCK-8 solution (Dojindo Laboratories, Inc.) was added to each well, followed by a 2-h incubation at 37˚C. Subsequently, absorbance was measured at 450 nm. The optimal ratio of $CD4^+$ T cells to IR-BNL CL.2 cells was determined based on changes in IR-BNL CL.2 cell viability across different co-culture ratios.

Glucose consumption assay. $CD4^+$ T cells from different treatment groups were co-cultured with IR-BNL CL.2 cells at the optimal cell ratio in phenol red-free DMEM for 24 h. At the end of the co-culture period, the supernatant was collected and glucose concentration was measured according to the instructions provided with the glucose assay kit (Beyotime Biotechnology). Glucose consumption was calculated as the difference between the initial glucose concentration and the glucose concentration in the supernatant after 24 h. The glucose degradation ratio was calculated as the percentage decrease in glucose consumption in the experimental group relative to the BNL CL.2 control group. Specifically, it was determined by subtracting the glucose consumption of the experimental group from that of the control group, dividing this difference by the glucose consumption of the control group, and multiplying by 100.

Superoxide dismutase (SOD) and malondialdehyde (MDA) assays. Following co-culture with $CD4^+$ T cells under the respective treatment conditions [the control (Con-T), model (Mod-T), PF40 (P-T), metformin (M-T) or PF40 + metformin (PM-T) groups], IR-BNL CL.2 cells from each treatment group were collected and washed three times with cold PBS. Cells were then lysed with an appropriate volume of RIPA lysis buffer (Thermo Fisher Scientific, Inc.) and incubating on ice for 15 min. The lysate was centrifuged at 12,000 x g for 10 min at 4˚C and the supernatant was collected for subsequent analysis. Protein concentrations were quantified using a BCA protein assay kit (cat. no. A045-4-2; Nanjing Jiancheng Bioengineering Institute) according to the manufacturer's protocol. The activity of SOD and levels of MDA were measured using respective commercial assay kits according to the manufacturer's protocol (SOD Assay Kit, cat. no. A001-3-2; MDA Assay Kit, cat. no. A003-1-2; both from Nanjing Jiancheng Bioengineering Institute).

Reactive oxygen species (ROS) assay. Treated IR-BNL CL.2 cells, following co-culture with $CD4^+$ T cells under the respective experimental conditions (Con-T, Mod-T, P-T, M-T or

PM-T), were collected and seeded into black, opaque-bottom 96-well plates for ROS detection. Cells were incubated for 24 h at 37˚C with 5% CO_2. Following adherence, the cells were washed twice with serum-free medium, and each well was loaded with 100 μM DCFDA in 1X buffer (cat. no. S0035S; Beyotime Biotechnology). After a 45-min incubation at 37˚C, the DCFDA solution was removed and the cells were washed twice with 1X PBS to minimize non-specific staining. The plate was then analyzed using a flow cytometer (NovoCyte), and data were collected and analyzed using NovoExpress software (version 1.4.1) according to the DCFDA kit protocol to quantify ROS levels (28).

Apoptosis assay. To evaluate apoptosis, IR-BNL CL.2 cells were collected and washed twice with cold PBS after co-culture with $CD4^+$ T cells under the indicated treatment conditions (Con-T, Mod-T, P-T, M-T or PM-T). Cells were resuspended in 1X binding buffer, and 5 μl Alexa Fluor™ 488 Annexin V and 1 μl 100 μg/ml propidium iodide were added as per the manufacturer's instructions (cat. no. A10788; Thermo Fisher Scientific, Inc.). The mixture was incubated in the dark at room temperature for 20 min to protect against photobleaching. Following incubation, the samples were analyzed immediately on a flow cytometer (NovoCyte), and data were collected and analyzed using NovoExpress software (version 1.4.1) to determine the proportions of live and apoptotic cells across treatment groups (29).

Western blot analysis. IR-BNL CL.2 cells were collected and washed three times with cold PBS following co-culture with $CD4^+$ T cells under the indicated treatment conditions (Con-T, Mod-T, P-T, M-T or PM-T). Cells were then lysed with RIPA lysis buffer containing protease inhibitors and lysates were incubated on ice for 30 min, vortexing every 10 min, to ensure complete lysis. Lysates were centrifuged at 12,000 x g for 10 min at 4˚C and the supernatant was collected for protein analysis. Protein concentrations were quantified using a BCA assay kit, and equal amounts of protein (30 μg/lane) from each sample were denatured at 95˚C for 5 min before being separated by SDS-PAGE on 10% gels. Following electrophoresis, the proteins were transferred onto PVDF membranes at 4˚C. Membranes were blocked with 5% BSA at room temperature for 1 h to minimize non-specific binding, and were then incubated overnight at 4˚C with rabbit monoclonal primary antibodies targeting p-PI3K (1:1,000), PI3K (1:1,000), p-AKT (1:500), AKT (1:500), p-IRS-1 (1:1,000), IRS-1 (1:1,000) and β-actin (1:5,000; cat. no. AC026; ABclonal Biotech Co., Ltd.). The following day, the membranes were washed three times with TBS-T buffer (TBS containing 0.1% Tween-20; 5 min each) to remove unbound antibodies, followed by incubation with HRP-conjugated goat anti-rabbit IgG (1:5,000; cat. no. 7074; Cell Signaling Technology, Inc.) for 1 h at room temperature. After washing, protein bands were visualized using a Pierce™ Fast Western kit (Thermo Fisher Scientific, Inc.) and images were captured. Band intensities were semi-quantified using Image Lab software (version 6.1.0; Bio-Rad Laboratories, Inc.).

Targeted energy metabolomics analysis by ultra performance liquid chromatography tandem mass spectrometry (UPLC-MS/MS). IR-BNL CL.2 cells were submitted to Wekemo Tech Co (https://www.bioincloud.tech/) for metabolomics analysis via UPLC-MS/MS. Briefly, 50 mg cell sample was mixed with 1,000 μl water/methanol/acetonitrile (1:2:2, v/v), vortexed for 25 min, and centrifuged at 14,000 x g for 15 min at 4˚C. The supernatant was dried using a vacuum centrifuge, and the residue was reconstituted in 100 μl 50% acetonitrile. The sample was centrifuged again at 14,000 x g for 15 min at 4˚C before undergoing UPLC-MS/MS analysis at Wekemo Tech Co. The conditions for mass spectrometry and chromatography are described in detail in the Supplementary materials.

Statistical analysis and visualization. Experimental data are presented as the mean ± standard deviation. Baseline data across treatment groups were analyzed using unpaired Student's t-test for comparisons between two groups or a one-way ANOVA for comparisons between multiple groups. Following one-way ANOVA, Tukey's post hoc multiple comparisons test was performed to determine significant differences between individual groups. $P<0.05$ was considered to indicate a statistically significant difference. Targeted energy metabolomics data analysis and visualization were performed on the Wekemo Bioincloud platform (https://bioincloud.tech/) using default parameters. To further explore metabolic differences between groups, principal component analysis (PCA), orthogonal partial least squares discriminant analysis (OPLS-DA) and redundancy analysis (RDA) were conducted on the same platform. Unless otherwise specified, all analyses were carried out with the standard settings provided by Wekemo Bioincloud.

Results

Physicochemical characterization of PF40. To investigate the physicochemical properties of PF40, a series of compositional and structural analyses were conducted. The polysaccharide yield from *Pseudostellaria heterophylla* was 18.63±1.21%. The total carbohydrate content of PF40 was determined to be 79.85±3.54%, while the protein content was relatively low at 0.12±0.01%, indicating a high degree of polysaccharide purity. Gel permeation chromatography revealed that PF40 exhibited a molecular weight distribution ranging from 52.6 to 212 kDa (Fig. S1), suggesting a heterogeneous macromolecular population. Monosaccharide composition was analyzed by HPLC after acid hydrolysis. The results showed that glucose was the predominant monosaccharide in PF40 (84.06 mol%), followed by a minor proportion of galactose (2.50 mol%). These findings were further supported by co-chromatography with standard monosaccharides and peak area comparison, as shown in the chromatograms. Fig. S2A presents the chromatograms of glucose and galactose standards, while Fig. S2B shows the monosaccharide composition analysis of PF40. These results indicated that PF40 is a polysaccharide mainly composed of glucose with a small amount of galactose.

Establishment of an IR-BNL CL.2 cell model. To establish an IR cell model, BNL CL.2 cells were treated with a high concentration of insulin. To determine the optimal insulin concentration, BNL CL.2 cells were exposed to insulin at concentrations ranging from $1x10^{-6}$ to $1x10^{-9}$ mol/l. As shown in Fig. 1A, compared with in the control group, the $1x10^{-7}$ to

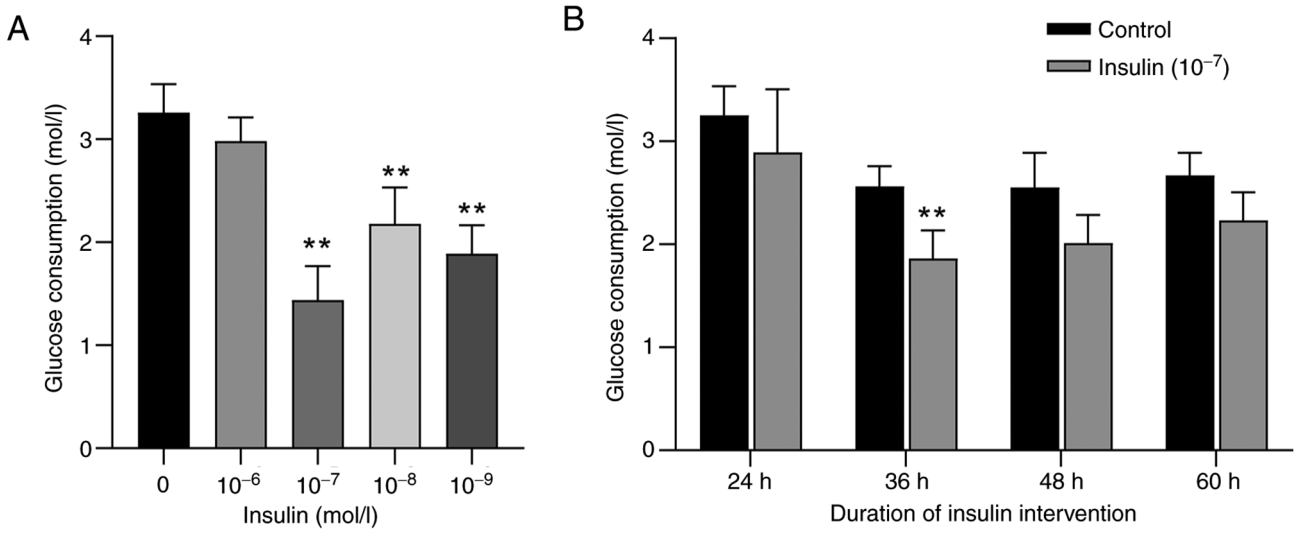

Figure 1. Effects of different insulin concentrations and intervention durations on glucose consumption in IR-BNL CL.2 cells. (A) Effects of various insulin concentrations (0-1x10^{-9} mol/l) on glucose consumption in IR-BNL CL.2 cells. **P<0.01 vs. untreated control group. (B) Effects of different intervention durations of insulin (1x10^{-7} mol/l) on glucose consumption in IR-BNL CL.2 cells. Data are presented as the mean ± SD, n=6. **P<0.01 vs. control group. IR-BNL CL.2, insulin-resistant BNL CL.2.

1x10^{-9} mol/l insulin-treated groups exhibited significantly inhibited glucose consumption in BNL CL.2 cells (P<0.01). The 1x10^{-7} mol/l insulin treatment exhibited the most pronounced inhibitory effect, reducing glucose consumption to 1.44±0.32 mol/l, which represents a 55.8% decrease from the control group (3.26±0.28 mol/l) (P<0.01). Therefore, 1x10^{-7} mol/l was selected as the optimal insulin concentration. Subsequently, the effects of varying exposure durations of 1x10^{-7} mol/l insulin on glucose consumption in cells was examined (Fig. 1B). Following treatment with 1x10^{-7} mol/l insulin for 24, 36, 48 and 60 h, glucose consumption decreased by 11.08, 27.11, 21.18 and 16.48%, respectively, compared with that in the control group, with a significant reduction observed at 36 h. These results indicated that treatment with 1x10^{-7} mol/l insulin for 36 h represented the optimal conditions for inducing insulin resistance in BNL CL.2 cells.

Notably, a non-linear relationship between insulin concentration and glucose consumption was observed in BNL CL.2 cells (Fig. 1). While low concentrations of insulin significantly promoted glucose uptake, higher concentrations did not further enhance glucose consumption and even showed a plateau or decline in effect. This may be due to insulin receptor desensitization, or negative feedback regulation induced by prolonged or excessive insulin exposure. At high doses, insulin can trigger signaling attenuation through mechanisms such as increased serine phosphorylation of IRS-1, thereby impairing downstream PI3K/AKT pathway activation and reducing glucose utilization efficiency. This phenomenon is consistent with previously reported insulin-induced insulin resistance in hepatocyte models (30).

Stability of the IR-BNL CL.2 model. To evaluate the stability of the insulin resistance cell model, IR-BNL CL.2 cells were continuously monitored following insulin treatment. As shown in Fig. 2B, compared with that in the control group, glucose consumption in cells pretreated with 1x10^{-7} mol/l insulin was significantly reduced at 36 and 48 h after insulin removal (P<0.01). Notably, at the final observation point of 60 h, although glucose consumption in the insulin-treated group remained lower than that in the control group, this difference was no longer statistically significant (P>0.05). This result suggested that the insulin resistance model remains stable for up to 48 h after insulin withdrawal but may begin to undergo partial self-repair by 60 h. Thus, subsequent experiments were performed within a 48-h time period following the establishment of the model.

Biocompatibility of T cells with IR-BNL CL.2. Isolated CD4$^+$ T cells (Fig. S3) were co-cultured with IR-BNL CL.2 cells at varying ratios (1:1, 2:1, 5:1, 10:1, 20:1 and 40:1) to assess the biocompatibility of the co-culture system. A CCK-8 assay was used to evaluate the viability of IR-BNL CL.2 cells (Fig. 2A). When the ratio of CD4$^+$ T cells was ≤10:1 there was no significant impact on IR-BNL CL.2 cell viability (P>0.05). However, at ratios of 20:1 and 40:1, the viability of IR-BNL CL.2 cells was significantly reduced (both P<0.01; 82.11 and 73.26% of the control group, respectively). Therefore, a CD4$^+$ T cell to IR-BNL CL.2 cell ratio of 10:1 was selected for subsequent experiments.

Glucose consumption of IR-BNL CL.2 cells in response to different CD4$^+$ T-cell treatments. CD4$^+$ T cells subjected to various treatments were co-incubated with IR-BNL CL.2 cells to assess their impact on glucose consumption in the IR-BNL CL.2 cells. As shown in Fig. 3, glucose consumption was significantly reduced in IR-BNL CL.2 cells compared with that in normal BNL CL.2 cells (P<0.05), confirming the successful establishment of the IR model. In the co-culture experiments, glucose consumption in IR-BNL CL.2 cells was markedly lower in the Mod-T group than in the Con-T group (P<0.01). Notably, co-culture of IR-BNL CL.2 cells with P-T, M-T or PM-T significantly improved glucose metabolism compared with the Mod-T group. The PM-T group showed the most pronounced effect, with glucose consumption nearly doubled compared with that in the Mod-T group (P<0.01).

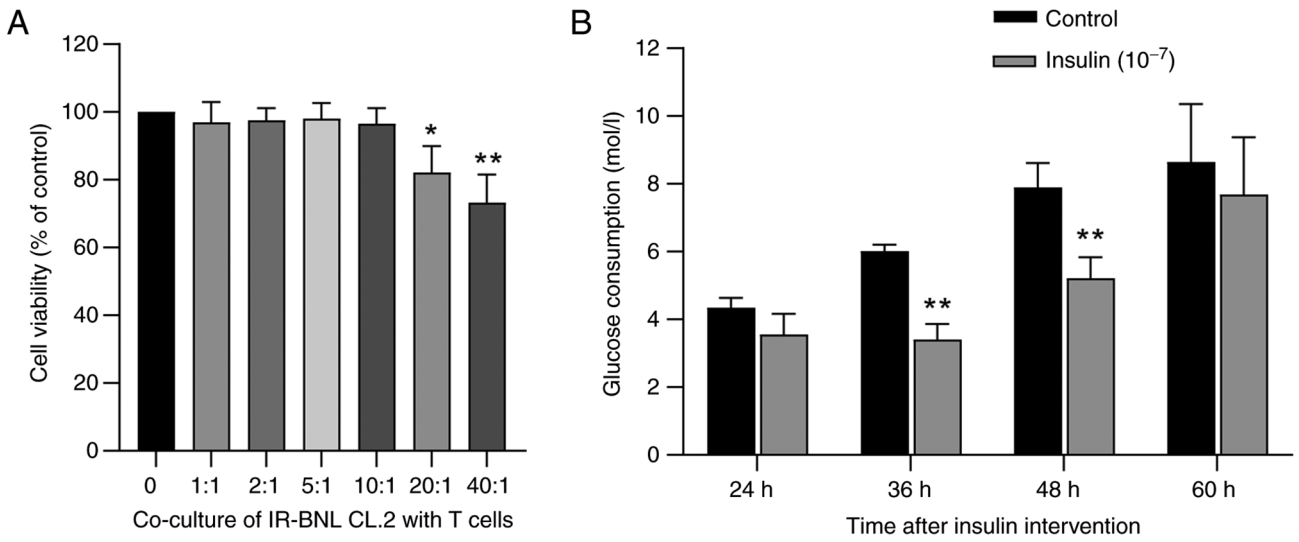

Figure 2. Stability of the IR-BNL CL.2 cell model and characteristics of co-culture with CD4+ T cells. (A) Analysis of cell viability in IR-BNL CL.2 and CD4+ T cells co-cultured at different ratios (1-40:1). (B) Changes in glucose consumption in IR-BNL CL.2 cells at various time points (24-60 h) following insulin intervention. **P<0.01 vs. control. Data are presented as the mean ± SD, n=6. *P<0.05, **P<0.01 vs. untreated IR-BNL CL.2 cells. IR-BNL CL.2, insulin-resistant BNL CL.2.

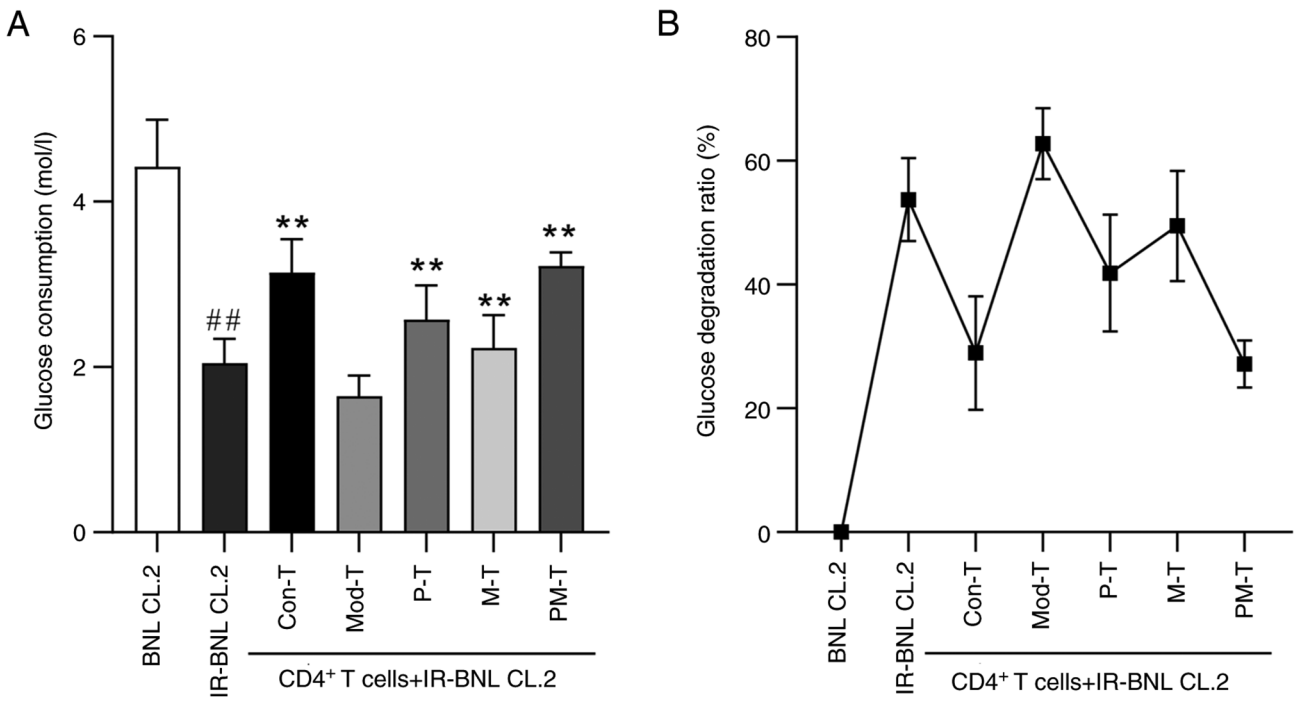

Figure 3. Effects of treated CD4+ T cells on glucose uptake of BNL CL-2 cells. (A) Glucose consumption in the different treatment groups. (B) Glucose degradation ratio in the different treatment groups. Data are presented as the mean ± SD, n=6. ##P<0.01 vs. BNL CL.2 control group; **P<0.01 vs. Mod-T group. IR-BNL CL.2, insulin-resistant BNL CL.2; Con-T, control; Mod-T, model; P-T, PF40; M-T, metformin; PM-T, combined PF40 and metformin.

Oxidative stress of IR-BNL CL.2 cells in response to different CD4+ T-cell treatments. To evaluate the oxidative stress status in IR-BNL CL.2 cells across different treatment groups, MDA levels and SOD activity were measured. MDA, a primary product of lipid peroxidation, reflects the extent of cellular oxidative damage, whereas SOD, a key antioxidant enzyme, indicates cellular antioxidant capacity (31). As shown in Fig. 4, MDA levels in IR-BNL CL.2 cells were significantly elevated in the Mod-T group compared with those in the Con-T group (P<0.01), whereas SOD activity was significantly reduced (P<0.01). Among the treatment groups, both the P-T and PM-T groups significantly lowered MDA levels (P<0.05), and although the M-T group also showed a trend toward reducing MDA, the difference was not statistically significant compared with the Mod-T group (P>0.05). All treatment groups exhibited notable improvements in SOD activity (P<0.01), with the PM-T group showing the most significant effect, nearly restoring SOD activity to control levels.

Subsequently, intracellular ROS levels in IR-BNL CL.2 cells co-cultured with CD4+ T cells from various treatment

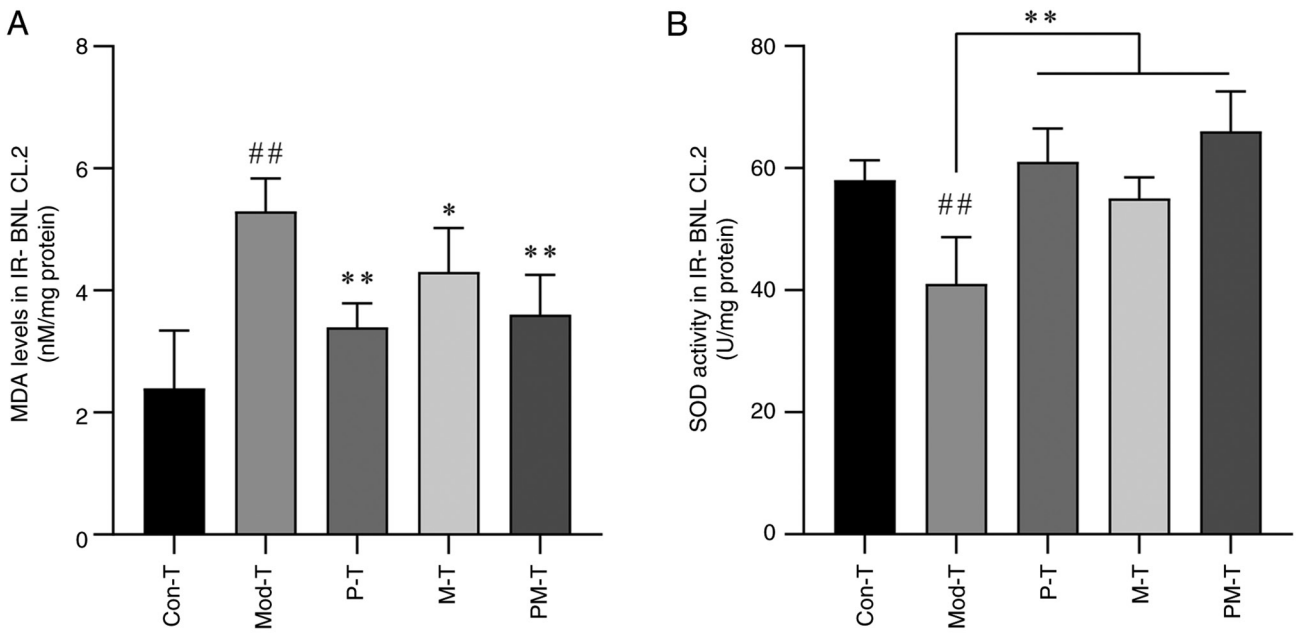

Figure 4. Effects of differently treated CD4+ T cells on (A) MDA and (B) SOD levels in IR-BNL CL.2 cells. Data are presented as the mean ± SD, n=5. ##P<0.01 vs. Con-T group; *P<0.05, **P<0.01 vs. Mod-T group. MDA, malondialdehyde; SOD, superoxide dismutase; IR-BNL CL.2, insulin-resistant BNL CL.2; Con-T, control; Mod-T, model; P-T, PF40; M-T, metformin; PM-T, combined PF40 and metformin.

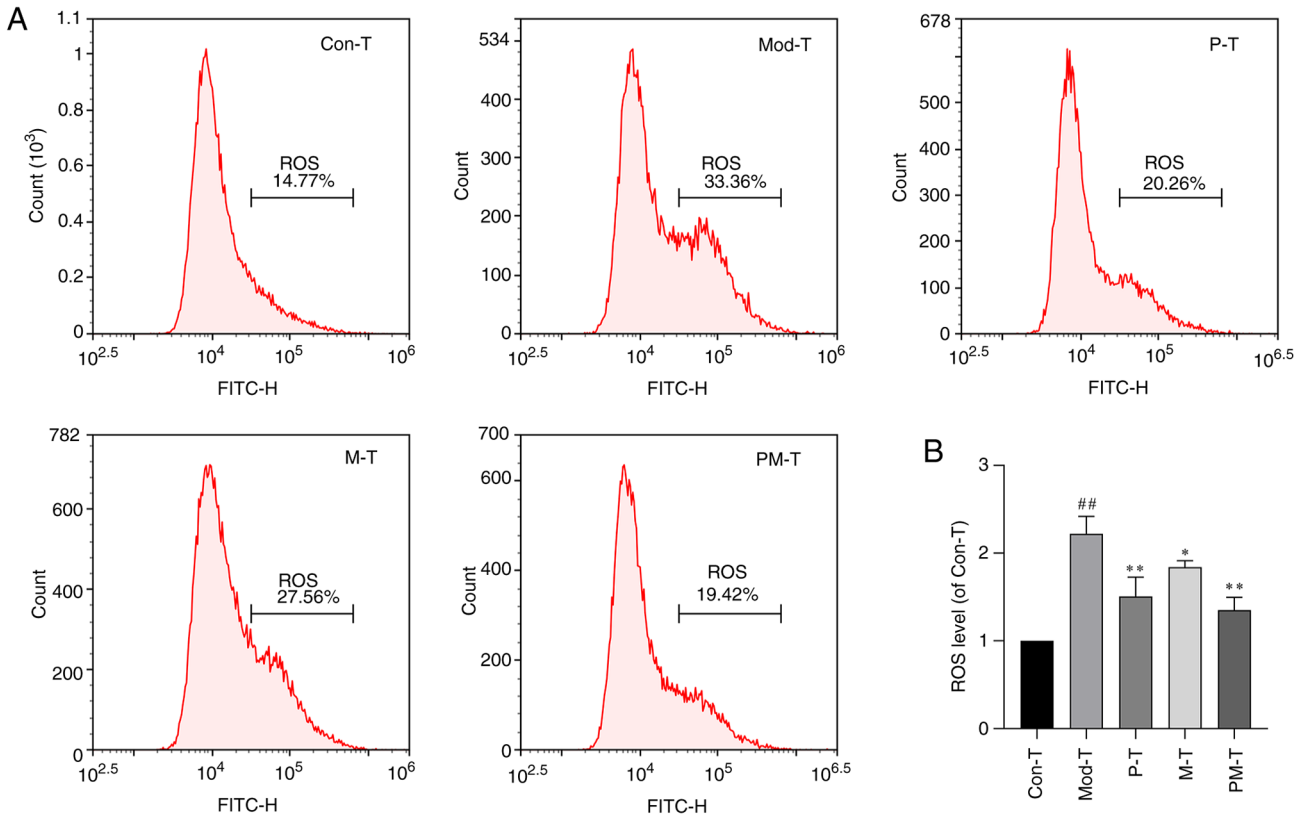

Figure 5. Effects of differently treated CD4+ T cells on ROS levels in IR-BNL CL.2 cells. (A) Representative ROS images for each treatment group. (B) Statistical analysis of ROS levels across treatment groups. Data are presented as the mean ± SD, n=6. ##P<0.01 vs. Con-T group; *P<0.05, **P<0.01 vs. Mod-T group. ROS, reactive oxygen species; IR-BNL CL.2, insulin-resistant BNL CL.2; Con-T, control; Mod-T, model; P-T, PF40; M-T, metformin; PM-T, combined PF40 and metformin.

groups were assessed using flow cytometry. As shown in Fig. 5, ROS levels were significantly elevated in the Mod-T group compared with those in the Con-T group (P<0.01), reaching approximately double that of the control levels. Both the P-T and M-T treatment groups significantly reduced ROS levels (P<0.05). Furthermore, the combined treatment group

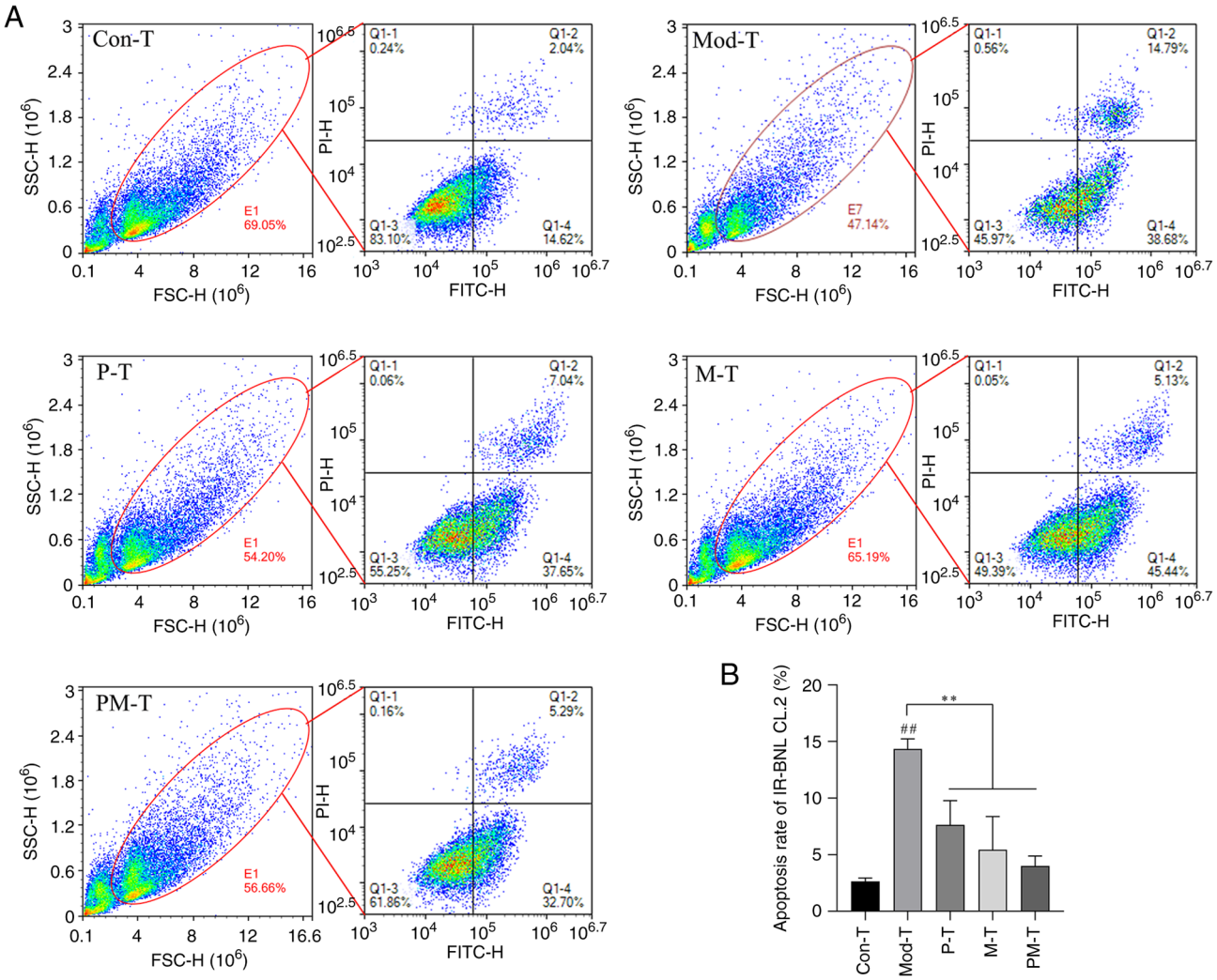

Figure 6. Effects of differently treated CD4⁺ T cells on the apoptosis of IR-BNL CL.2 cells. (A) Representative plots of apoptosis in each treatment group. (B) Quantification of apoptosis levels across treatment groups, based on the percentages of cells in the Q1-2 quadrants as determined by flow cytometry. Data are presented as the mean ± SD, n=6. ##P<0.01 vs. Con-T group; **P<0.01 vs. Mod-T group. IR-BNL CL.2, insulin-resistant BNL CL.2; Con-T, control; Mod-T, model; P-T, PF40; M-T, metformin; PM-T, combined PF40 and metformin.

(PM-T) exhibited the strongest inhibitory effect on ROS levels, restoring them to close to the control levels (P<0.01).

Apoptosis of IR-BNL CL.2 cells in response to different CD4⁺ T-cells treatments. FSC (forward scatter) and SSC (side scatter) plots were used to assess cell populations, where FSC reflects cell size and SSC indicates cell granularity or internal complexity. To investigate the impact of CD4⁺ T cells from different treatment groups on IR-BNL CL.2 cell apoptosis, the apoptotic rate of IR-BNL CL.2 cells in the co-culture system was measured using flow cytometry (Fig. 6). The results showed that the Mod-T group exhibited significantly increased apoptosis of IR-BNL CL.2 cells compared with that in the Con-T group (P<0.01). This finding indicated that CD4⁺ T cells in a T2DM state may exacerbate insulin resistance by promoting the apoptosis of IR-BNL CL.2 cells. Following P-T or M-T treatment, the apoptosis rates in IR-BNL CL.2 cells were significantly reduced (P<0.01). Notably, the PM-T group showed the most pronounced protective effect, reducing the rate of apoptosis to close to that of control levels (P<0.01). These findings suggested that PF40 and metformin may mitigate apoptosis in IR-BNL CL.2 cells through functional modulation of CD4⁺ T cells, with a potential synergistic effect.

Expression of IRS-1/PI3K/AKT and phosphorylated proteins in IR-BNL CL.2 cells. The expression of insulin signaling markers in IR-BNL CL.2 cells was assessed using western blot analysis (Fig. 7). The results indicated that in the Mod-T group IR-BNL CL.2 cells exhibited an impaired insulin signaling cascade, as evidenced by increased phosphorylation of IRS-1^{Ser307} (P<0.01), and significantly decreased phosphorylation of PI3K$^{p58\text{-}Tyr607}$ and AKT^{S473} (both P<0.01), compared with that in the Con-T group. By contrast, the PM-T group showed a marked reduction in p-IRS-1^{Ser307} (P<0.01), and a significant increases in p-PI3K$^{p58\text{-}Tyr607}$ and p-AKT^{S473} levels (P<0.01) compared with in the Mod-T group. These findings suggested that P-T or M-T may activate the PI3K/AKT signaling pathway by reducing p-IRS-1^{Ser307} expression, effectively increasing insulin sensitivity and improving insulin resistance.

Energy metabolism in IR-BNL CL.2 cells in response to different CD4⁺ T-cell treatments. UPLC-MS/MS was used

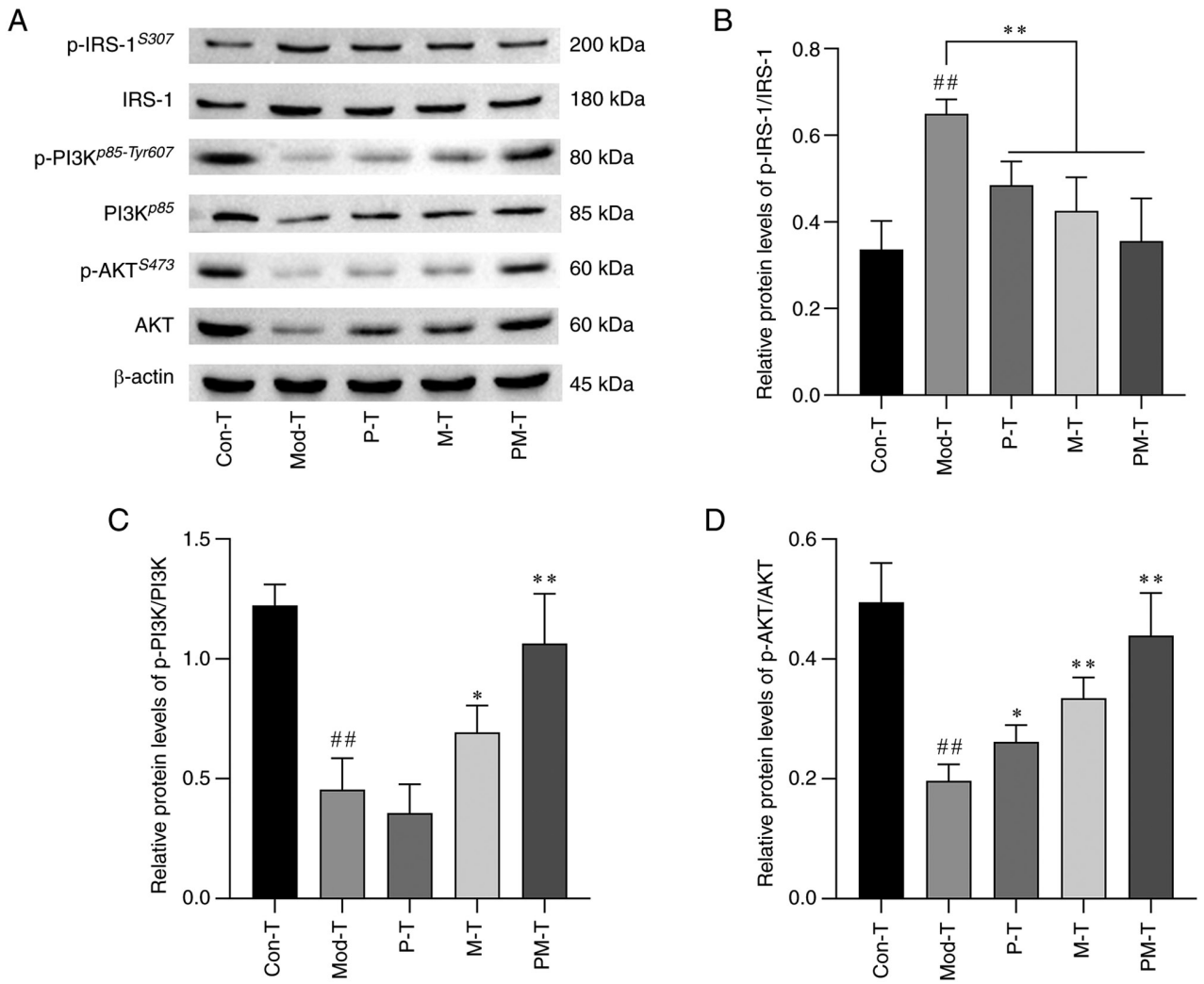

Figure 7. Effects of differently treated CD4+ T cells on the IRS-1/PI3K/AKT signaling pathway in IR-BNL CL.2 cells. (A) Representative western blot images showing protein and p-protein expression levels of IRS-1, PI3K and AKT across the different treatment groups. Relative protein expression levels of (B) p-IRS-1/IRS-1, (C) p-PI3K/PI3K, and (D) p-AKT/AKT. Data are presented as the mean ± SD, n=3. ##P<0.01 vs. Con-T group; *P<0.05, **P<0.01 vs. Mod-T group. Con-T, control; Mod-T, model; P-T, PF40; M-T, metformin; PM-T, combined PF40 and metformin; IRS-1, insulin receptor substrate-1; p-, phosphorylated.

to investigate changes in energy metabolism-related metabolites in IR-BNL CL.2 cells. To streamline data analysis, the Con-T, Mod-T and PM-T groups were selected. To explore metabolic differences between samples, PCA and OPLS-DA were performed (Fig. 8A-C). The PCA score plot indicated a clear separation trend among the three groups on PC1 (57.9%) and PC2 (12.1%). The OPLS-DA analysis between the Con-T and Mod-T groups showed that the predictive component T score and orthogonal component T score explained 42.1 and 25.3% of the variance, respectively. In the OPLS-DA analysis between the Mod-T and PM-T treatment groups, the predictive component T score and orthogonal component T score explained 69.3 and 9.6% of the variance, respectively. Both OPLS-DA score plots displayed good group separation, indicating significant metabolic alterations due to insulin resistance modeling, while PM-T treatment effectively modulated these metabolic abnormalities.

As shown in Fig. 8D and F, heatmaps illustrated the levels of key metabolites involved in the tricarboxylic acid (TCA) cycle and glycolysis pathways within IR-BNL CL.2 cells. Compared with in the Con-T group, the Mod-T group exhibited significant changes in key metabolites within the TCA cycle and glycolysis. In the TCA cycle, α-ketoglutarate, succinate, fumarate and malic acid levels were markedly increased, while oxaloacetate levels were markedly decreased. In the glycolysis pathway, levels of D-glucose-6-phosphate and β-D-fructose-6-phosphate were substantially reduced in the Mod-T group. These results suggested that the Mod-T group may compensate for impaired glycolysis by upregulating key metabolites in the TCA cycle to maintain cellular energy balance. The PM-T treatment group an opposing metabolic pattern was detected compared with that in the Mod-T group, particularly regarding levels of α-ketoglutarate and D-glucose-6-phosphate, suggesting that PM-T exerts therapeutic effects by modulating the metabolic balance between the TCA cycle and glycolysis pathways.

RDA showed that the first and second axes explained 64.43 and 16.54% of the total variance, respectively (Fig. 8E). The RDA ordination plot revealed clear separation among the Con-T, Mod-T and PM-T groups. RDA revealed that the Mod-T group was positively associated with ROS and apoptosis rate, whereas the PM-T group was positively associated with SOD

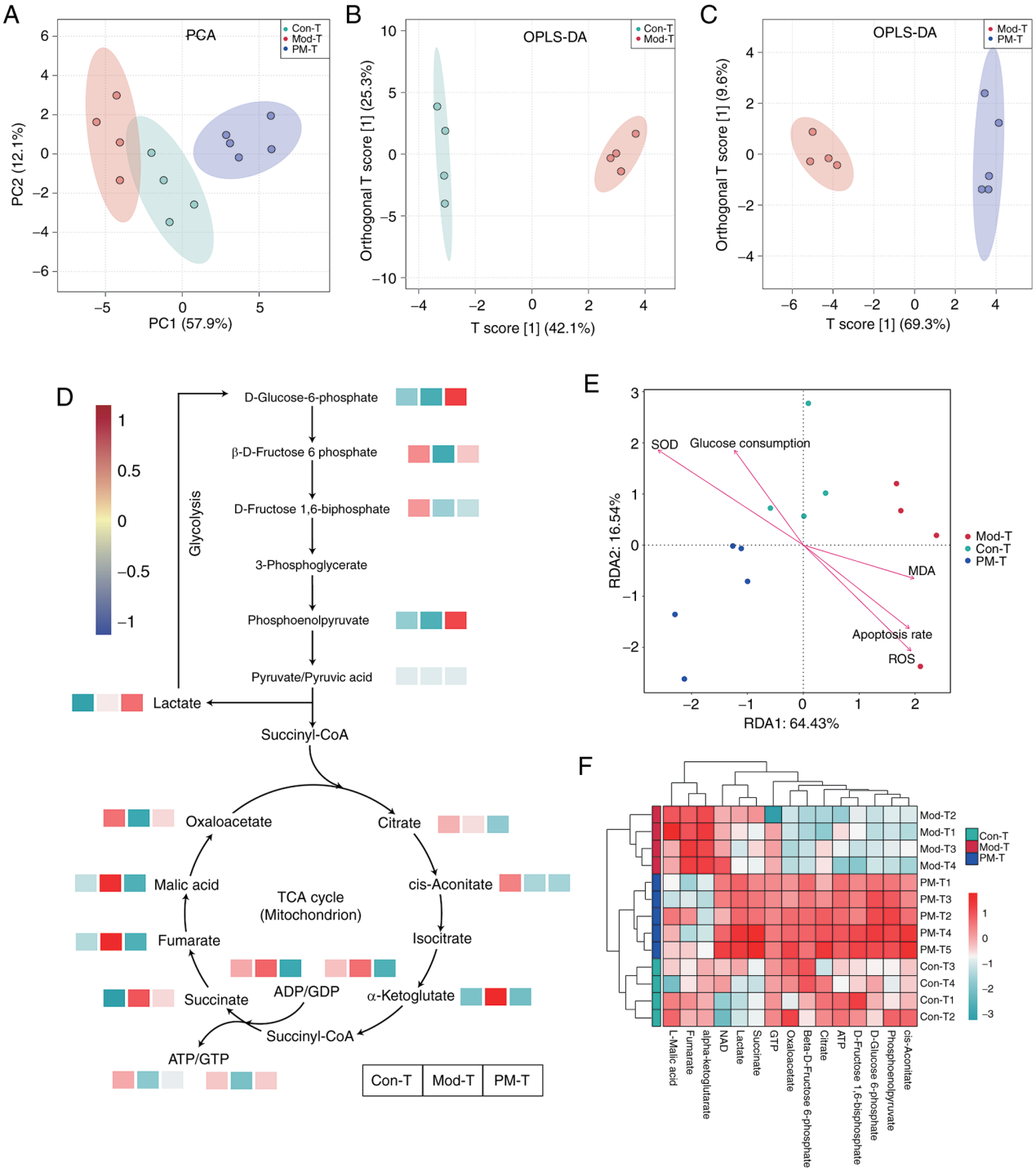

Figure 8. Targeted energy metabolomics analysis of the different treatment groups. (A) PCA of metabolites in the different treatment groups. OPLS-DA was performed between the (B) Con-T and Mod-T groups, and the (C) Mod-T and PM-T groups. (D) Heat maps showing the relative content of key glycolysis products across different treatment groups. (E) Redundancy analysis. Data are presented as the mean ± SD, n=4 or 5. (F) Heat map showing the relative content of key TCA cycle products across different treatment groups. Mod-T. Con-T, control; Mod-T, model; P-T, PF40; M-T, metformin; PM-T, combined PF40 and metformin; PCA, principal component analysis; OPLS-DA, orthogonal partial least squares discriminant analysis; TCA, tricarboxylic acid.

activity and negatively with MDA levels, indicating that PM-T treatment improves oxidative stress by enhancing antioxidant capacity and reducing lipid peroxidation damage.

Discussion

In the present study, an IR-BNL CL.2 cell model was established and co-incubated with intestinal CD4$^+$ T cells treated with PF40, metformin or both. The results showed that P-T reduced oxidative stress in IR-BNL CL.2 cells by lowering ROS and MDA levels, while enhancing SOD activity, which reflected improved antioxidant defense. Oxidative stress is a known factor in insulin resistance, primarily by affecting glucose metabolism and the insulin signaling pathways, thereby accelerating the progression of insulin resistance (31). By mitigating oxidative stress, P-T co-culture restored the

redox balance and improved insulin sensitivity. The findings of the present study emphasized that $CD4^+$ T cells may serve a critical role in alleviating insulin resistance in IR-BNL CL.2 cells. This aligns with accumulating evidence that immune cells, particularly $CD4^+$ T lymphocytes, notably impact metabolic activity and inflammation in the context of insulin resistance (32,33).

The liver is a key organ involved in glucose metabolism and a primary target in insulin resistance (34,35). Establishing a stable and reliable IR cell model is crucial for screening anti-insulin resistance drugs and studying their mechanisms of action. Murine embryonic liver cells are widely used as model cells to investigate hepatic insulin resistance, and insulin serves as an inducer for developing IR cell models (36,37). In developing the IR-BNL CL.2 cell model, a marked reduction in glucose consumption in response to optimal induction conditions was observed ($1x10^{-7}$ mol/l insulin for 36 h), and model stability was confirmed over 48 h. Impaired glucose consumption and elevated oxidative stress levels in IR-BNL CL.2 cells are consistent with previous findings, validating the stability and reliability of the model (36,38). When co-cultured with P-T cells, glucose uptake was restored in IR-BNL CL.2 cells. The present study also investigated the biocompatibility of $CD4^+$ T cells with IR-BNL CL.2 cells at specific co-culture ratios, and the results showed that the optimal non-cytotoxic ratio for co-culturing $CD4^+$ T cells with IR-BNL CL.2 cells was 10:1. The establishment of this co-culture system provides a basis for further exploration of the mechanisms by which $CD4^+$ T cells modulate insulin resistance in IR-BNL CL.2 cells.

In the current study, the murine hepatocyte-derived BNL CL.2 cell line was selected to establish an insulin resistance model for co-culture with $CD4^+$ T cells isolated from PF40-treated rats with T2DM. This choice was made to maintain taxonomic proximity within the Rodentia order and to minimize potential immune incompatibility or non-specific activation that could result from co-culturing rodent-derived immune cells with more distantly related species. While BNL CL.2 cells are embryonic in origin and do not fully recapitulate the metabolic complexity of human hepatocytes, they are widely used in studies of hepatic insulin signaling (39), oxidative stress (40) and energy metabolism (41). Nevertheless, the limitations of this model in mimicking human pathophysiology should be acknowledged, and future studies incorporating humanized hepatocyte-immune co-culture systems or liver organoids will be necessary to validate and extend the findings in a translational context. Moreover, the T cell-to-hepatocyte ratio employed in the co-culture system (10:1) exceeds physiological levels typically found *in vivo*. This elevated ratio was selected based on the biocompatibility testing of different $CD4^+$ T cell/IR-hepatocyte ratios, to ensure that $CD4^+$ T cells could exert sufficient paracrine and immunomodulatory effects on IR hepatocytes without inducing excessive cytotoxicity. While this setup enhances the detection of immunometabolic interactions *in vitro*, it may not fully replicate the cellular microenvironment of the gut-liver axis under physiological or pathological conditions. Therefore, the data should be interpreted as proof-of-concept findings, and future studies employing more physiologically relevant cell ratios or three-dimensional co-culture models are warranted to confirm the observed effects.

SOD is a critical antioxidant enzyme that effectively scavenges superoxide anions, thereby reducing oxidative stress-induced cellular damage. In the pathophysiology of T2DM, prolonged hyperglycemic conditions lead to a marked elevation in intracellular ROS levels, exacerbating oxidative stress, which further exacerbates insulin resistance and cellular injury (42,43). P-T intervention significantly increased SOD activity in IR-BNL CL.2 cells in the present study, suggesting that P-T alleviated oxidative stress by enhancing cellular antioxidant capacity. Furthermore, the observed reduction in MDA levels supports the antioxidant role of P-T. As a marker of lipid peroxidation, decreased MDA levels indicate that P-T may reduce lipid peroxidation under IR conditions, thereby lowering the risk of oxidative membrane damage. Lipid peroxidation, a consequence of oxidative stress, destabilizes cell membranes, increases permeability and impairs cell function (44). Compared with in the Mod-T group, the P-T group exhibited a significant reduction in MDA levels, suggesting that P-T may serve a crucial role in inhibiting lipid peroxidation and preserving membrane integrity.

Oxidative stress is one of the primary inducers of cellular apoptosis, with ROS acting as reactive molecules that cause oxidative damage to membrane lipids, proteins and DNA under oxidative stress, ultimately triggering apoptotic pathways (45). In the present study, P-T treatment significantly reduced ROS levels in IR-BNL CL.2 cells, along with a decrease in the lipid peroxidation marker MDA. This finding indicated that P-T not only exhibits antioxidant properties but may also inhibit the progression of oxidative damage by reducing ROS. Apoptosis assays of IR-BNL CL.2 cells further validated these findings, with Mod-T showing substantial apoptosis relative to the Con-T group, whereas P-T treatment significantly reduced apoptotic cell counts. Thus, P-T may prevent apoptosis pathway activation by lowering oxidative stress, which is crucial for mitigating insulin resistance-associated cellular injury.

To further elucidate the potential molecular mechanisms by which P-T influenced glucose metabolism, the expression of insulin signaling-related markers in IR-BNL CL.2 cells was examined. Upon binding to its receptor, insulin promotes glucose uptake through a series of signaling cascades, resulting in the phosphorylation of IRS proteins at multiple tyrosine residues, which subsequently activate downstream molecules such as PI3K and AKT (46). The PI3K/AKT pathway is a primary regulator of metabolic functions and glucose uptake induced by insulin (46-48). Activated AKT serves a central role in regulating various downstream pathways, including those involved in cell proliferation, protein synthesis and glucose metabolism. Phosphorylation of AKT further activates GLUT4, enhancing glucose uptake in peripheral tissues. IRS-1, a major IRS subtype, is closely associated with glucose homeostasis in the liver; however, phosphorylation of IRS-1 at the Ser307 residue significantly diminishes its activity, which is linked to the inhibition of insulin signaling (49,50). Western blot analysis showed that in the Mod-T group, levels of p-IRS-1^{Ser307} were markedly elevated, whereas $PI3K^{p85\text{-}Tyr607}$ and p-AKT^{Ser473} levels were notably reduced, indicating impairment of the insulin signaling cascade. Treatment with P-T or M-T significantly reduced p-IRS-1^{Ser307} levels, enhanced $PI3K^{p85\text{-}Tyr607}$ expression, and increased AKT phosphorylation, thereby promoting glucose uptake.

Phosphorylation of AKT has a pivotal role in glucose uptake and utilization by activating key glycolytic enzymes, such as glucokinase, which facilitates glucose phosphorylation, an essential step for entry into glycolysis and the TCA cycle (51,52). During a state of insulin resistance, reduced AKT phosphorylation may lead to decreased glucokinase activity, directly lowering the levels of glucose-6-phosphate (53). In the present study, reduced glucose-6-phosphate levels were observed in the Mod-T group. This reduction disrupted the TCA cycle, which could impair glycolytic input, resulting in decreased ATP production efficiency and subsequent ROS accumulation. In the IR-BNL CL.2 model group, elevated ROS levels and reduced TCA cycle intermediates suggested mitochondrial stress, compromising cellular bioenergetics and promoting apoptosis. This increase in apoptosis aligned with the results from RDA, where elevated ROS and lipid peroxidation were associated with higher apoptotic rates. Thus, disruption of the glucokinase-AKT pathway highlights links among glucose metabolism disorders, oxidative stress and cell survival.

The present study used targeted energy metabolomics analysis to reveal differences in energy metabolism pathways in IR-BNL CL.2 cells among the different treatment groups. In the Mod-T group, a notable increase in multiple key metabolites within the TCA cycle was observed, particularly α-ketoglutarate, succinate, fumarate and malic acid, which suggested the presence of a compensatory regulatory mechanism in response to metabolic dysregulation. Studies have shown that the accumulation of TCA cycle metabolites is often associated with mitochondrial dysfunction (54,55). Concurrently, the significant reduction of glycolytic intermediates (such as D-glucose-6-phosphate and β-D-fructose-6-phosphate) in the Mod-T group suggested that glycolysis may be suppressed. This metabolic shift aligns with previously reported characteristics of metabolic disease models (56). Notably, the PM-T treatment group exhibited metabolic features that were the opposite of those in the Mod-T group. Following PM-T treatment, the levels of glycolytic intermediates, such as D-glucose-6-phosphate and phosphoenolpyruvate, were increased, and TCA cycle metabolites approached normal levels. This finding suggested that PM-T may improve cellular energy metabolism by modulating the metabolic balance between the TCA cycle and glycolysis pathways.

RDA provided further biochemical evidence supporting the role of PM-T in ameliorating oxidative stress. The separation between the Mod-T and PM-T groups on the RDA plot, along with the positive association between the Mod-T group and elevated ROS levels and apoptosis rates, indicated that Mod-T-induced metabolic stress may be associated with increased oxidative damage. However, PM-T treatment showed a strong positive association with SOD activity and a negative association with MDA content, indicating enhanced antioxidant defense capacity and reduced lipid peroxidation in treated cells. This transition in oxidative status may represent a key mechanism by which PM-T reduces cellular stress and prevents apoptosis. Collectively, PM-T may exert its protective effects through rebalancing energy metabolism and enhancing antioxidant responses, potentially alleviating functional impairments in IR cells.

The combined treatment of $CD4^+$ T cells with PF40 and metformin demonstrated synergistic effects on antioxidant activity and apoptosis inhibition. Compared with M-T, the PM-T group exhibited markedly enhanced antioxidant capacity and reduced ROS levels, which may be attributed to the complementary mechanisms of PF40 and metformin. PF40 primarily reduces oxidative stress through its antioxidant properties, whereas metformin improves cellular metabolism by modulating the insulin signaling pathway (10,57). Thus, their combined application may alleviate insulin resistance and improve cell status through several different mechanisms. Although metformin is effective in reducing insulin resistance, adjunct therapy with natural antioxidants may further enhance therapeutic outcomes and potentially reduce side effects associated with metformin monotherapy (57,58). It has been reported that mushroom polysaccharide NAP-3 can enhance the efficacy of metformin in lipid and glucose metabolism in mice with T2DM by reshaping the homeostasis of the gut microbiota community (59). The *Astragalus* polysaccharide APS-D1 has also been shown to reduce the required dosage of metformin by enriching *Staphylococcus lentus*, which promotes fatty acid oxidation and inhibits gluconeogenesis (60).

In the present study, the effects of differentially treated intestinal immune cell subsets on insulin resistance were investigated. The results revealed that modulating the homeostasis of $CD4^+$ T cells in the gut immune system may notably improve insulin signaling and glucose metabolism in an IR cell model. This aligns with previous studies highlighting the role of gut immune cells in metabolic regulation, particularly the exacerbation of IR by T-cell alterations in inflammatory environments (61,62). Targeting intestinal immune cells may present a novel approach for the prevention and treatment of insulin resistance and metabolic diseases (63). However, the $CD4^+$ T-cell population in the present study likely includes various subsets, such as Th1, Th2 and Th17 cells, and Tregs. The specific roles of these subsets in this process remain unclear. To further elucidate this mechanism, future studies should employ techniques such as single-cell sequencing to better understand the contributions of these immune cell subsets in improving insulin resistance and reducing apoptosis.

In our previous study, the regulatory effects of PF40 on $CD4^+$ T-cell subsets, particularly in the balance between Tregs and Th17 cells were determined (11). PF40 may alleviate immune system overactivation and reduce insulin resistance by enhancing the function of Tregs. Tregs serve a critical role in maintaining immune tolerance and suppressing excessive immune responses, whereas Th17 cells are typically associated with inflammatory responses and the development of insulin resistance (3,4). By modulating the Treg/Th17 balance, PF40 may inhibit Th17 cell expansion and reduce the inflammation induced by these cells, thereby improving insulin signaling. Specifically, PF40 may enhance the secretion of factors such as IL-10 by Tregs, while suppressing the secretion of IL-17A by Th17 cells, thereby regulating the immune microenvironment and mitigating insulin resistance caused by immune activation (11). In the present study, it was observed that P-T cells suppressed oxidative stress responses and activated the IRS-1/PI3K/AKT signaling pathway. These findings not

only provide evidence for the potential mechanisms through which PF40 maintains immune balance but also highlight its promising application prospects in the treatment of insulin resistance.

While the current study provides experimental data on the role of PF40 in alleviating insulin resistance, its limitations must be considered. First, the present study primarily relied on *in vitro* models, and although the IR-BNL CL.2 cell model has been widely validated in insulin resistance research, it differs from *in vivo* environments, particularly regarding the dynamic changes in immune cells and tissue-specific responses. Therefore, future studies should consider validating these findings in animal models to enhance the biological relevance of the results. Second, since the study did not delve deeply into the specific mechanisms of $CD4^+$ T-cell subsets, future research could employ single-cell sequencing technologies or other high-throughput analysis methods to explore the roles and interactions of different T-cell subsets in insulin resistance. These studies would contribute to a more comprehensive understanding of PF40-mediated modulation of the immune system and provide novel insights and strategies for the treatment of insulin resistance and related metabolic diseases. Finally, although the combined treatment of PF40 and metformin indicated potential synergistic effects, the absence of formal synergy calculations represents a limitation of the present study, and further quantitative analyses are warranted to substantiate this interaction.

The present study provides evidence that P-T cells are conducive to improving immune activation-induced insulin resistance. However, the precise mechanisms by which PF40 regulates $CD4^+$ T-cell subset differentiation remain to be elucidated. It is well known that polysaccharides are characterized by their high molecular weight and low bioavailability. Our previous research identified a water-soluble pectic polysaccharide isolated from *Pseudostellaria heterophylla* that can be absorbed through the intestinal mucosa and enter the systemic circulation (12). Emerging evidence has suggested that fermentation of *Porphyra haitanensis* polysaccharides by *Lactiplantibacillus plantarum* markedly reduces their particle size and enhances the anti-allergic effects both *in vitro* and *in vivo* (21). Fucoidan has also been shown to markedly modulate the composition and functional output of the gut microbiota (64,65). Notably, this microbial remodeling appears to be a key mechanism underpinning the biological activity of polysaccharides. The reshaped microbiota ferments these complex carbohydrates, leading to the production of critical metabolites, particularly short-chain fatty acids (SCFAs), such as acetate, propionate and butyrate (66). These SCFAs act as essential signaling molecules and energy substrates, serving pivotal roles in the differentiation of intestinal immune cells (67).

In conclusion, the present study demonstrated that P-T cells significantly enhanced SOD activity, reduced MDA and ROS levels, and lowered oxidative stress, thereby reducing apoptosis in the IR-BNL CL.2 cell model. Additionally, these T cells alleviated insulin resistance by activating the IRS-1/PI3K/AKT signaling pathway, increasing glucose uptake in IR-BNL CL.2 cells, and optimizing the TCA cycle and glycolysis. $CD4^+$ T lymphocytes in intestinal tissue serve a critical role in PF40-mediated metabolic regulation and are key effector cells in the action of PF40 in improving insulin resistance. Targeted modulation of intestinal immune cell homeostasis may represent a promising strategy for the prevention and treatment of insulin resistance.

Acknowledgements

The authors would like to thank Dr Bianhong Zhang (Fujian Agriculture and Forestry University, Fuzhou, China) for their help in data visualization of targeted energy metabolism. The authors would also like to thank Dr Ye Liu (Fujian Agriculture and Forestry University, Fuzhou, China) for assisting in the detection of targeted energy metabolism.

Funding

This study was funded by the National Natural Science Foundation of China (grant nos. 82405034, 81872994 and 81903945), a major scientific and technological innovation project of Fujian University of Traditional Chinese Medicine (grant no. XJB2022001), the Key Laboratory of Traditional Chinese Medicine in Medical Institutions of Fujian Province (Fujian University of Traditional Chinese Medicine), the Construction Project of Quality Evaluation System for *Pseudostellaria heterophylla* in Zherong County Pharmaceutical Development Center (2024), and the Science and Technology Innovation Special Fund of Fujian Agriculture and Forestry University (grant no. CXZX2020037A).

Availability of data and materials

The metabolomics data generated in the present study may be found in the OMIX, China National Center for Bioinformation/Beijing Institute of Genomics, Chinese Academy of Sciences database under accession number OMIX010841 or at the following URL: https://ngdc.cncb.ac.cn/omix/release/OMIX010841. The other data generated in the present study may be requested from the corresponding author.

Authors' contributions

YK and YL conceived and designed the experiments. YH, LZ, JC and WP analyzed and interpreted the data. YK wrote the manuscript. WL contributed to statistical analysis and manuscript revision, and JH contributed to experimental design and manuscript revision. YK and YL confirm the authenticity of all the raw data. All authors read and approved the final version of the manuscript.

Ethics approval and consent to participate

The present study was approved by the Institutional Animal Care and Use Committee at Fujian Academy of Chinese Medical Sciences (Fuzhou, China; approval no. FJATCM-IAEC2020002).

Patient consent for publication

Not applicable.

Competing interests

The authors declare that they have no competing interests.

References

1. Garg SS, Kushwaha K, Dubey R and Gupta J: Association between obesity, inflammation and insulin resistance: Insights into signaling pathways and therapeutic interventions. Diabetes Res Clin Pract 200: 110691, 2023.
2. Guzmán-Flores J, Ramírez-Emiliano J, Pérez-Vázquez V and López-Briones S: Th17 and regulatory T cells in patients with different time of progression of type 2 diabetes mellitus. Cent Eur J Immunol 45: 29-36, 2020.
3. Kiernan K and MacIver NJ: A novel mechanism for Th17 inflammation in human type 2 diabetes mellitus. Trends Endocrinol Metab 31: 1-2, 2020.
4. Zhang S, Gang X, Yang S, Cui M, Sun L, Li Z and Wang G: The alterations in and the role of the Th17/Treg balance in metabolic diseases. Front Immunol 12: 678355, 2021.
5. Yan JB, Luo MM, Chen ZY and He BH: The function and role of the Th17/Treg cell balance in inflammatory bowel disease. J Immunol Res 2020: 8813558, 2020.
6. Lin Z, Zhang J, Duan T, Yang J and Yang Y: Trefoil factor 3 can stimulate Th17 cell response in the development of type 2 diabetes mellitus. Sci Rep 14: 10340, 2024.
7. Hu DJ, Shakerian F, Zhao J and Li SP: Chemistry, pharmacology and analysis of Pseudostellaria heterophylla: A mini-review. Chin Med 14: 21, 2019.
8. Lu F, Yang H, Lin SD, Zhao L, Jiang C, Chen ZB, Liu YY, Kan YJ, Hu J and Pang WS: Cyclic peptide extracts derived from pseudostellaria heterophylla ameliorates COPD via regulation of the TLR4/MyD88 pathway proteins. Front Pharmacol 11: 850, 2020.
9. Kan Y, Liu Y, Huang Y, Zhao L, Jiang C, Zhu Y, Pang Z, Hu J, Pang W and Lin W: The regulatory effects of Pseudostellaria heterophylla polysaccharide on immune function and gut flora in immunosuppressed mice. Food Sci Nutr 10: 3828-3841, 2022.
10. Hu J, Pang W, Chen J, Bai S, Zheng Z and Wu X: Hypoglycemic effect of polysaccharides with different molecular weight of Pseudostellaria heterophylla. BMC Complement Altern Med 13: 267, 2013.
11. Liu Y, Kan Y, Huang Y, Jiang C, Zhao L, Hu J and Pang W: Physicochemical characteristics and antidiabetic properties of the polysaccharides from pseudostellaria heterophylla. Molecules 27: 3719, 2022.
12. Chen J, Pang W, Kan Y, Zhao L, He Z, Shi W, Yan B, Chen H and Hu J: Structure of a pectic polysaccharide from pseudostellaria heterophylla and stimulating insulin secretion of INS-1 cell and distributing in rats by oral. Int J Biol Macromol 106: 456-463, 2018.
13. Brucklacher-Waldert V, Carr EJ, Linterman MA and Veldhoen M: Cellular plasticity of CD4+ T cells in the intestine. Front Immunol 5: 488, 2014.
14. Jiménez JM, Contreras-Riquelme JS, Vidal PM, Prado C, Bastías M, Meneses C, Martín AJM, Perez-Acle T and Pacheco R: Identification of master regulator genes controlling pathogenic CD4+ T cell fate in inflammatory bowel disease through transcriptional network analysis. Sci Rep 14: 10553, 2024.
15. Tao L, Liu H and Gong Y: Role and mechanism of the Th17/Treg cell balance in the development and progression of insulin resistance. Mol Cell Biochem 459: 183-188, 2019.
16. Wang M, Chen F, Wang J, Zeng Z, Yang Q and Shao S: Th17 and Treg lymphocytes in obesity and type 2 diabetic patients. Clin Immunol 197: 77-85, 2018.
17. Monteiro-Sepulveda M, Touch S, Mendes-Sá C, André S, Poitou C, Allatif O, Cotillard A, Fohrer-Ting H, Hubert EL, Remark R, *et al*: Jejunal T cell inflammation in human obesity correlates with decreased enterocyte insulin signaling. Cell Metab 22: 113-124, 2015.
18. Garidou L, Pomié C, Klopp P, Waget A, Charpentier J, Aloulou M, Giry A, Serino M, Stenman L, Lahtinen S, *et al*: The gut microbiota regulates intestinal CD4 T cells expressing RORγt and controls metabolic disease. Cell Metab 22: 100-112, 2015.
19. Zi C, He L, Yao H, Ren Y, He T and Gao Y: Changes of Th17 cells, regulatory T cells, Treg/Th17, IL-17 and IL-10 in patients with type 2 diabetes mellitus: A systematic review and meta-analysis. Endocrine 76: 263-272, 2022.
20. Wei Y, Jing J, Peng Z, Liu X and Wang X: Acacetin ameliorates insulin resistance in obesity mice through regulating Treg/Th17 balance via MiR-23b-3p/NEU1 axis. BMC Endocr Disorders 21: 57, 2021.
21. Cheng Z, Wang SH, Li LY, Zhou YC and Zhang CY: Fermented Porphyra haitanensis polysaccharides inhibit the degranulation of mast cell and passive cutaneous anaphylaxis. Food & Medicine Homology 3: 9420086, 2025.
22. Bradford MM: A rapid and sensitive method for the quantitation of microgram quantities of protein utilizing the principle of protein-dye binding. Anal Biochem 72: 248-254, 1976.
23. Cai M, Xing H, Tian B, Xu J, Li Z, Zhu H, Yang K and Sun P: Characteristics and antifatigue activity of graded polysaccharides from Ganoderma lucidum separated by cascade membrane technology. Carbohydr Polym 269: 118329, 2021.
24. Nataraj A, Govindan S, Ramani P, Subbaiah KA, Sathianarayanan S, Venkidasamy B, Thiruvengadam M, Rebezov M, Shariati MA, Lorenzo JM and Pateiro M: Antioxidant, anti-tumour, and anticoagulant activities of polysaccharide from calocybe indica (APK2). Antioxidants (Basel) 11: 1694, 2022.
25. Kim E, Tran M, Sun Y and Huh JR: Isolation and analyses of lamina propria lymphocytes from mouse intestines. STAR Protoc 3: 101366, 2022.
26. Hu X, Yu Q, Hou K, Ding X, Chen Y, Xie J, Nie S and Xie M: Regulatory effects of Ganoderma atrum polysaccharides on LPS-induced inflammatory macrophages model and intestinal-like Caco-2/macrophages co-culture inflammation model. Food Chem Toxicol 140: 111321, 2020.
27. da Rocha GH, Müller C, Przybylski-Wartner S, Schaller H, Riemschneider S and Lehmann J: AhR-induced anti-inflammatory effects on a Caco-2/THP-1 co-culture model of intestinal inflammation are mediated by PPARγ. Int J Mol Sci 25: 13072, 2024.
28. Liu X, Xiang D, Jin W, Zhao G, Li H, Xie B and Gu X: Timosaponin B-II alleviates osteoarthritis-related inflammation and extracellular matrix degradation through inhibition of mitogen-activated protein kinases and nuclear factor-κB pathways in vitro. Bioengineered 13: 3450-3461, 2022.
29. Wang W, Huang S, Li S, Li X, Ling Y, Wang X, Zhang S, Zhou D and Yin W: Rosa sterilis juice alleviated breast cancer by triggering the mitochondrial apoptosis pathway and suppressing the Jak2/Stat3 pathway. Nutrients 16: 2784, 2024.
30. Fan X, Tao J, Zhou Y, Hou Y, Wang Y, Gu D, Su Y, Jang Y and Li S: Investigations on the effects of ginsenoside-Rg1 on glucose uptake and metabolism in insulin resistant HepG2 cells. Eur J Pharmacol 843: 277-284, 2019.
31. Tangvarasittichai S: Oxidative stress, insulin resistance, dyslipidemia and type 2 diabetes mellitus. World J Diabetes 6: 456-480, 2015.
32. Liu L, Hu J, Wang Y, Lei H and Xu D: The role and research progress of the balance and interaction between regulatory T cells and other immune cells in obesity with insulin resistance. Adipocyte 10: 66-79, 2021.
33. Wu H and Ballantyne CM: Metabolic inflammation and insulin resistance in obesity. Circ Res 126: 1549-1564, 2020.
34. Sakurai Y, Kubota N, Yamauchi T and Kadowaki T: Role of insulin resistance in MAFLD. Int J Mol Sci 22: 4156, 2021.
35. Tanase DM, Gosav EM, Costea CF, Ciocoiu M, Lacatusu CM, Maranduca MA, Ouatu A and Floria M: The intricate relationship between type 2 diabetes mellitus (T2DM), insulin resistance (IR), and nonalcoholic fatty liver disease (NAFLD). J Diabetes Res 2020: 3920196, 2020.
36. Schafer A, Neschen S, Kahle M, Sarioglu H, Gaisbauer T, Imhof A, Adamski J, Hauck SM and Ueffing M: The epoxyeicosatrienoic acid pathway enhances hepatic insulin signaling and is repressed in insulin-resistant mouse liver. Mol Cell Proteomics 14: 2764-2774, 2015.
37. Zhou X, Wang LL, Tang WJ and Tang B: Astragaloside IV inhibits protein tyrosine phosphatase 1B and improves insulin resistance in insulin-resistant HepG2 cells and triglyceride accumulation in oleic acid (OA)-treated HepG2 cells. J Ethnopharmacol 268: 113556, 2021.
38. Zhong RF, Liu CJ, Hao KX, Fan XD and Jiang JG: Polysaccharides from Flos Sophorae Immaturus ameliorates insulin resistance in IR-HepG2 cells by co-regulating signaling pathways of AMPK and IRS-1/PI3K/AKT. Int J Biol Macromol 280: 136088, 2024.
39. Jiang S, Wu X, Wang Y, Zou J and Zhao X: The potential DPP-4 inhibitors from Xiao-Ke-An improve the glucolipid metabolism via the activation of AKT/GSK-3β pathway. Eur J Pharmacol 882: 173272, 2020.

40. Kim S, Yoon D, Lee YH, Lee J, Kim ND, Kim S and Jung YS: Transformation of liver cells by 3-methylcholanthrene potentiates oxidative stress via the downregulation of glutathione synthesis. Int J Mol Med 40: 2011-2017, 2017.
41. Jobgen WS and Wu G: L-Arginine increases AMPK phosphorylation and the oxidation of energy substrates in hepatocytes, skeletal muscle cells, and adipocytes. Amino Acids 54: 1553-1568, 2022.
42. Ding W, Yang X, Lai K, Jiang Y and Liu Y: The potential of therapeutic strategies targeting mitochondrial biogenesis for the treatment of insulin resistance and type 2 diabetes mellitus. Arch Pharm Res 47: 219-248, 2024.
43. Roden M, Petersen KF and Shulman GI: Insulin resistance in type 2 diabetes. In: Textbook of Diabetes Wiley, pp 238-249, 2024.
44. Masenga SK, Kabwe LS, Chakulya M and Kirabo A: Mechanisms of oxidative stress in metabolic syndrome. Int J Mol Sci 24: 7898, 2023.
45. Redza-Dutordoir M and Averill-Bates DA: Activation of apoptosis signalling pathways by reactive oxygen species. Biochim Biophys Acta 1863: 2977-2992, 2016.
46. Chen H, Li J, Zhang Y, Zhang W, Li X, Tang H, Liu Y, Li T, He H, Du B, *et al*: Bisphenol F suppresses insulin-stimulated glucose metabolism in adipocytes by inhibiting IRS-1/PI3K/AKT pathway. Ecotoxicol Environ Saf 231: 113201, 2022.
47. Zhao SL, Liu D, Ding LQ, Liu GK, Yao T, Wu LL, Li G, Cao SJ, Qiu F and Kang N: Schisandra chinensis lignans improve insulin resistance by targeting TLR4 and activating IRS-1/PI3K/AKT and NF-κB signaling pathways. Int Immunopharmacol 142: 113069, 2024.
48. Huang L, Guo Z, Huang M, Zeng X and Huang H: Triiodothyronine (T3) promotes browning of white adipose through inhibition of the PI3K/AKT signalling pathway. Sci Rep 14: 20370, 2024.
49. Báez AM, Ayala G, Pedroza-Saavedra A, González-Sánchez HM and Amparan LC: Phosphorylation codes in IRS-1 and IRS-2 are associated with the activation/inhibition of insulin canonical signaling pathways. Curr Issues Mol Biol 46: 634-649, 2024.
50. Woo JR, Bae SH, Wales TE, Engen JR, Lee J, Jang H and Park S: The serine phosphorylations in the IRS-1 PIR domain abrogate IRS-1 and IR interaction. Proc Nat Acad Sci USA 121: e2401716121, 2024.
51. Lien EC, Lyssiotis CA and Cantley LC: Metabolic reprogramming by the PI3K-Akt-mTOR pathway in cancer. Metabolism in Cancer 207: 39-72, 2016.
52. Fontana F, Giannitti G, Marchesi S and Limonta P: The PI3K/Akt pathway and glucose metabolism: A dangerous liaison in cancer. Int J Biol Sci 20: 3113-3125, 2024.
53. Park J, Rho HK, Kim KH, Choe SS, Lee YS and Kim JB: Overexpression of Glucose-6-Phosphate dehydrogenase is associated with lipid dysregulation and insulin resistance in obesity. Mol Cell Biol 25: 5146-5157, 2005.
54. Martínez-Reyes I and Chandel NS: Mitochondrial TCA cycle metabolites control physiology and disease. Nat Commun 11: 102, 2020.
55. Choi I, Son H and Baek JH: Tricarboxylic Acid (TCA) cycle intermediates: Regulators of immune responses. Life (Basel) 11: 69, 2021.
56. Zhang X, Jia Y, Yuan Z, Wen Y, Zhang Y, Ren J, Ji P, Yao W, Hua Y and Wei Y: Sheng Mai San ameliorated heat stress-induced liver injury via regulating energy metabolism and AMPK/Drp1-dependent autophagy process. Phytomedicine 97: 153920, 2022.
57. Tian JL, Si X, Shu C, Wang YH, Tan H, Zang ZH, Zhang WJ, Xie X, Chen Y and Li B: Synergistic effects of combined anthocyanin and metformin treatment for hyperglycemia in vitro and in vivo. J Agric Food Chem 70: 1182-1195, 2022.
58. Namvarjah F, Shokri-Afra H, Moradi-Sardareh H, Khorzoughi RB, Pasalar P, Panahi G and Meshkani R: Chlorogenic acid improves anti-lipogenic activity of metformin by positive regulating of AMPK signaling in HepG2 cells. Cell Biochem Biophys 80: 537-545, 2022.
59. Sun L, Jiang J, Zeng Y, Zhu J, Wang S, Huang D and Cao C: Polysaccharide NAP-3 synergistically enhances the efficiency of metformin in type 2 diabetes via Bile Acid/GLP-1 axis through gut microbiota remodeling. J Agric Food Chem 72: 21077-21088, 2024.
60. Long J, Li M, Yao C, Ma W, Liu H and Yan D: Structural characterization of Astragalus polysaccharide-D1 and its improvement of low-dose metformin effect by enriching Staphylococcus lentus. Int J Biol Macromol 272: 132860, 2024.
61. Toubal A, Kiaf B, Beaudoin L, Cagninacci L, Rhimi M, Fruchet B, da Silva J, Corbett AJ, Simoni Y, Lantz O, *et al*: Mucosal-associated invariant T cells promote inflammation and intestinal dysbiosis leading to metabolic dysfunction during obesity. Nat Commun 11: 3755, 2020.
62. Khan S, Luck H, Winer S and Winer DA: Emerging concepts in intestinal immune control of obesity-related metabolic disease. Nat Commun 12: 2598, 2021.
63. Riedel S, Pheiffer C, Johnson R, Louw J and Muller CJF: Intestinal barrier function and immune homeostasis are missing links in obesity and type 2 diabetes development. Front Endocrinol (Lausanne) 12: 833544, 2021.
64. Wang YX, Chen XL, Zhou K, Wang LL, Zhong YZ, Peng J, Ge BS, Ho CT and Lu CY: Fucoidan dose-dependently alleviated hyperuricemia and modulated gut microbiota in mice. Food & Medicine Homology 3: 9420095, 2025.
65. Qin W, Wei B, Ren P, Chang Y, Xue C and Tang Q: Fucoidan from Apostichopus japonicus enhances intestinal barrier function and promotes intestinal immunity via regulating the gut microbiota and tryptophan metabolism. Int J Biol Macromol 301: 139929, 2025.
66. Zhang Y, Ji W, Qin H, Chen Z, Zhou Y, Zhou Z, Wang J and Wang K: Astragalus polysaccharides alleviate DSS-induced ulcerative colitis in mice by restoring SCFA production and regulating Th17/Treg cell homeostasis in a microbiota-dependent manner. Carbohydr Polym 349: 122829, 2025.
67. Yang W, Yu T, Huang X, Bilotta AJ, Xu L, Lu Y, Sun J, Pan F, Zhou J, Zhang W, *et al*: Intestinal microbiota-derived short-chain fatty acids regulation of immune cell IL-22 production and gut immunity. Nat Commun 11: 4457, 2020.